Wide Bandgap Semiconductor Based High Performance Bidirectional Resonant Converter for Electric Vehicle Application

Conference Paper · February 2022

DOI: 10.1109/ICAEEE54957.2022.9836379

2 authors:

Md. Tanvir Shahed
Bangladesh University of Engineering and Technology

ABM Harun-ur Rashid
Bangladesh University of Engineering and Technology

Wide Bandgap Semiconductor Based High Performance Bidirectional Resonant Converter for Electric Vehicle Application

Md. Tanvir Shahed[1, 2, *], A.B.M. Harun-Ur Rashid[1]
[1]Department of Electrical and Electronic Engineering, Bangladesh University of Engineering and Technology, Dhaka-1000
[2]Department of Electrical and Electronic Engineering, Uttara University, Dhaka-1230
[*]Email: tanvirshahed1996@gmail.com

Abstract—**In this paper, a bidirectional capacitor-inductor-inductor-inductor-capacitor (CLLLC) resonant converter based on a wide bandgap (WBG) transistor is designed and analyzed at MHz-level switching frequency to accomplish high power density and high efficiency. A discrete-time Proportional-Integral-Derivative (PID) controller based on phase shifted pulse width modulation (PWM) technique has been developed for the closed-loop control of the aforementioned CLLLC converter. The converter is designed with WBG switching devices to accomplish fast switching with minimal switching losses, and it is also compared to Si-based switching devices. For the proper thermal design of the converter, a precise power loss model of the switching devices has been developed. A 5 kW CLLLC converter with 400-450V DC input and 250-465V DC output with an operating frequency of 1 MHz has been designed and simulated under a variety of loading conditions. The maximum conversion efficiency achieved with Gallium Nitride (GaN)-based devices was 97.2 percent in forward mode and 97 percent in reverse mode.**

Keywords— WBG, GaN transistors, Bidirectional, CLLLC, DC-DC converter, electric vehicle, EV, Electric Vehicle, high power density, high frequency, MHz, high efficiency.

I. INTRODUCTION

Bidirectional Direct current–direct current (DC-DC) converters play an important role in a variety of applications, including electric vehicles (EVs), DC power distribution systems, renewable energy systems, aerospace power supplies, industrial systems, and uninterruptible power supply (UPS) that require bidirectional power transmission [1]–[4]. This type of high-power bidirectional DC-DC resonant converter can achieve DC voltage variation as well as electrical isolation. Fig. 1 depicts a block schematic of a typical EV onboard charger, which includes an AC-DC power factor correction (PFC) stage and a DC-DC converter [5]. To accomplish unity PFC and AC to DC conversion, The PFC stage connects with the AC grid and a DC link capacitor. To attain voltage and current regulation as well as galvanic isolation, the bidirectional DC-DC converter links between the DC link capacitor and a battery pack. Dual active bridge (DAB) [6], [7] and CLLLC [8]–[11] converters have attracted substantial attention among the existing DC-DC converter topologies because of their simple and symmetric architecture on both sides of the high frequency (HF) transformer. The fundamental benefit of DAB architecture over a CLLLC resonant converter is the absence of resonant capacitors that must withstand high voltage stresses. The CLLLC converter, on the other hand, has the capability of accomplishing soft-switching under practically any loading scenario. These converter switches can achieve zero voltage switching (ZVS) on the inverter side and zero current switching (ZCS) on the rectification side without the use of an auxiliary circuit, allowing it to operate at higher switching frequencies.

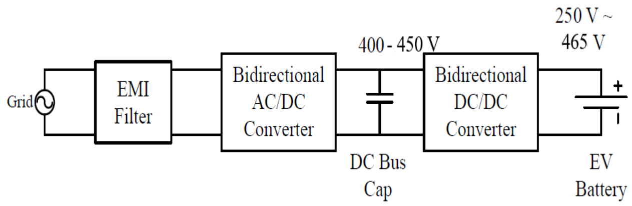

Fig. 1 Block Schematic of Typical EV On-board Charger.

Moreover, for switching converters, passive storage components occupy a significant portion of the overall size. Higher switching frequency operation is, without a doubt, the most obvious technique for reducing the size of magnetic components. Nevertheless, even partial hard-switching at any switching device at a higher switching frequency could result in significant switching losses, resulting in significant efficiency degradation as well as increased thermal management burden. As a result, unlike a DAB converter, this paper, which concentrates primarily on EV on-board charger applications, employs the CLLLC architecture as a more viable alternative for HF DC-DC conversion with no additional control complexity necessary to enable soft-switching.

Due to the recent popularity of the CLLLC converter and its widespread application prospects, various research works have been conducted to enhance the performance of CLLLC converters for a variety of applications. For example, in [11], a novel operation mode analysis has been established to synthesize the optimal tank parameters for a given set of conditions. In [12], it is demonstrated that raising the switching frequency from 65 kHz to 1 MHz lessens the overall size of capacitors and inductors by approximately 50%, facilitating the building of high-power-density resonant converters. Zong *et el.* [13] have developed a double voltage rectification (DVR) modulation technique to broaden the operation voltage range of bidirectional resonant converters by providing a step-up voltage gain. Chu *et el.* [14] have proposed a method for significantly reducing common-mode (CM) electromagnetic interference (EMI) noise caused by CLLLC converter. As a result, CM chokes can be downsized, and converter power density can be improved. On the other hand, different open-loop soft-start techniques for CLLLC Bi-directional Resonant Converters have been proposed in [15] to minimize current and voltage burden during starting.

Furthermore, as semiconductor technology advances, third-generation wide-bandgap semiconductor devices, such as gallium nitride (GaN) devices and silicon carbide (SiC) devices, have been invented to assist Bidirectional converters in achieving higher frequency, higher power density, and higher efficiency by supplanting traditional devices such as Si MOSFETs and IGBTs. An overview of some major material properties of these devices is provided. in [16]. Based on the comparison data, it can be concluded that GaN offers the highest breakdown voltage, bandgap, and electron velocity properties, making it an excellent choice for high voltage and high-frequency applications. Even though GaN's thermal conductivity is lower than that of SiC, GaN devices can offer a high power-density design with effective cooling methods. Furthermore, GaN devices offer smaller gate charge and on-resistance than Si and SiC devices, leading to reduced switching charges and faster switching transitions. In addition, faster switching transitions result in lower switching loss. GaN also has a lower output capacitance, which leads to lower switching loss and simpler realization of zero voltage switching (ZVS). GaN 2D Electron Gas (2DEG) can conduct in the third quadrant, alleviating the need for an anti-parallel diode, which is required in other Si and SiC-based devices. As a result, it has zero reverse recovery loss, which leads to lower switching loss and less EMI noise. So, GaN FETs can maintain high efficiency during high-frequency operation among the available switching devices.

In this context, this work focuses on designing an efficient Bidirectional CLLLC resonant converter with high performance based on various switching devices. For efficiency calculations, a precise power loss model of the switching devices was used. A discrete-time PID controller based on the phase-shifted PWM technique has been developed to regulate the output voltage and govern the bidirectional power conversions. During the simulation, the designed converter was tested for various switching device models from various manufacturers, with E-mode GaN High Electron Mobility Transistor (HEMT) from GaN System providing the highest efficiency compared to other switching devices.

II. Operation Principle of Bidirectional CLLLC Converter

Fig. 2 depicts the structure of a bidirectional CLLLC converter. The converter can transfer power in both directions, which are referred to as charging mode (Grid to vehicle (G2V)) and discharging mode (Vehicle to grid (V2G)). This CLLLC converter is made up of two full-bridge converters with a total of eight switches. In order to achieve inversion, the S14 and S23 switches are turned on at 50% duty cycle in the forward direction. With their antiparallel diodes, S58, S67 will achieve rectification. Anti-parallel diodes are not required when GaN transistors are used as switching devices because they are naturally capable of reverse conduction. Anti-parallel diodes are only required for reverse conduction in Si, SiC MOSFETs, and IGBTs.

The CLLLC resonant converter has six stages in one operation period. The driving circuit's operational scenarios are the same in both forward and reverse directions, and the resonant elements are also symmetrical in both directions. As a result, the operating principles of the converter are essentially the same in both directions, and only one operating direction needs to be examined. A detailed analysis regarding the forward operation principle can be found in [17], so it will not be analyzed in this paper. Analyzing the operational processes reveals that the CLLC resonant converter can accomplish ZVS on primary side switches and ZCS on secondary side switches. At low loads, the converter can end up losing soft switching, which can be solved by selecting appropriate resonant and magnetizing inductances in the converter.

III. Design of Bidirectional CLLLC Converter

Design of the converter comprises determining the turns ratio of the transformer (n), designing of magnetizing inductance (L_m), resonant inductances (L_1 and L_2), capacitances (C_1 and C_2), and designing of phase-shifted PWM based discrete-time PID controller.

A. Design of Transformer Turns Ratio

At the self-resonant frequency f_r, resonant converters have the highest efficiency. Thus, the converter should work at this frequency under normal working conditions. Turns ratio of the transformer can then be calculated as,

$$\mathrm{n} = \frac{N_1}{N_2} = \frac{V_{in\_nom}}{V_{o\_nom}} \quad (1)$$

where $N_1, N_2, V_{in\_nom}, V_{o\_nom}$ denotes the transformer primary and secondary turns ratio, nominal input, and output voltage respectively.

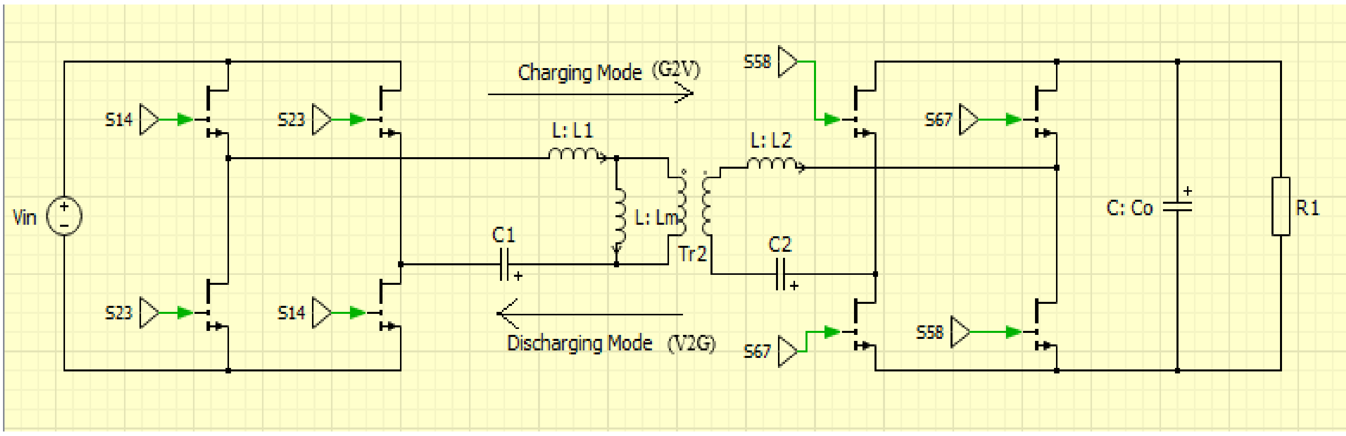

Fig. 2. The Structure of Bidirectional CLLLC Resonant Converter

B. Design of Resonant Parameters

Fig. 3 shows the equivalent circuits of the CLLLC converter in both directions. The resonant tank is made up of L_1, L_2, L_m, C_1, and C_2 and its self-resonant frequency is given by the following equation:

$$f_r = \frac{1}{\sqrt{L_1 C_1}} = \frac{1}{\sqrt{L_2 C_2}} \qquad (2)$$

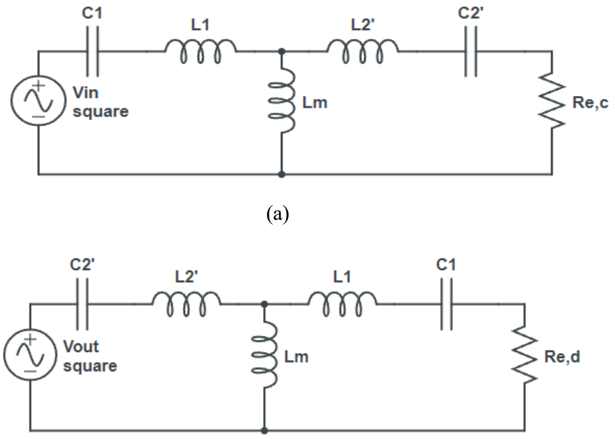

(a)

(b)

Fig. 3. Equivalent circuit of the CLLLC converter in (a) G2V mode and (b) V2G mode.

$Re,\ C_2',L_2'$ are the equivalent $R_o,\ C_2,\ L_2$ of the CLLLC converters, correspondingly. Here, R_o denotes the output load resistance of the converter. The equivalent load resistance is calculated utilizing the First Harmonic Approximation (FHA). For the charging mode, the equivalent load resistance(Re,c), inductance (L_2'), and capacitance (C_2') of the converter can be computed as follows:

$$Re,c = \frac{8n^2}{\pi^2} R_o \quad L_2' = n^2 L_2 \quad C_2' = \frac{C_2}{n^2} \qquad (3)$$

Similarly, the parameters for the discharging mode will be as follows:

$$Re,d = \frac{8}{n^2\pi^2} R_o \quad L_2' = \frac{L_2}{n^2} \quad C_2' = n^2 C_2 \qquad (4)$$

ZVS in primary-side switches can be ensured by maintaining the current through these switches negative at the time of turn-on. During the dead-time, the primary current should be able to fully charge and discharge the output capacitors of the primary switches. The magnitude of this current is determined by the magnetizing inductance and the deadtime duration. As a result, the magnetizing inductance (L_m), output capacitance of switches (C_{oss}), operating frequency, and dead-time (t_{dead}) control the ZVS on the primary side switches. During dead time, this converter operates similarly to an LLC resonant converter [18]. As a result, the magnetizing inductance can then be expressed similarly to that of the full-bridge LLC resonant converter. This expression is as follows:

$$L_m \leq \frac{t_{dead}}{16 C_{oss} f_{s,max}} \qquad (5)$$

where $f_{s,max}$ denotes the highest switching frequency.

A quite low magnetizing inductance, L_m ensures ZVS in primary-side switches under all variety of load conditions. L_m, on the other hand, cannot be too low. The magnetizing current would be extremely high due to too low L_m, leading to massive conduction losses, higher peak voltage requirements of the primary side capacitor, as well as higher apparent power requirements of switches. A high magnetizing inductance results in a lower magnetizing current, but it restricts the voltage gain of the converter. As a result, the magnetizing inductance cannot be excessively high.

The ZVS range is also affected by the dead-time between switches. Higher dead-time will aid in accomplishing ZVS for a wide range of input and output voltages. Furthermore, by increasing the magnetizing inductance with a long dead-time, the magnetizing current can be minimized. Higher dead-time, on the other hand, will result in a high primary RMS current due to no energy transfer during the dead-time period. When determining the magnetizing inductance, L_m, all of these parameters must be taken into account. All of these possible factors should be considered when calculating the magnetizing inductance, L_m.

C. Design of Phase Shifted PWM based Discrete-time PID Controller

The block diagram of the proposed discrete-time PID controller based on phase-shift PWM is given in the following:

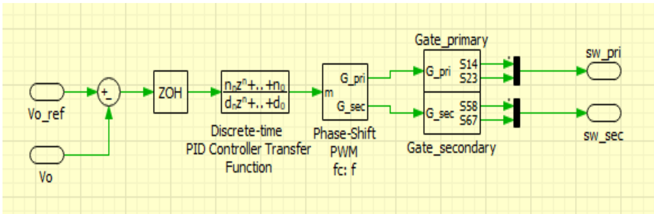

Fig. 4. PID Controller Block Diagram

The controller is made up of three major blocks: the Zero Order Hold block, the Discrete-time PID Controller Transfer Function block, and the Phase Shift PWM block. The Zero Order Hold block samples and holds the difference signal between the reference and actual output voltage level. The Discrete-time PID Controller block then performs proportional, integral, and derivative control to stabilize the output voltage. The transfer function of a discrete-time PID controller in the Z domain can be represented by the following equation:

$$C(z) = K_p + \frac{K_i T_s z}{z-1} + \frac{K_d N(z-1)}{(1+NT_s)z - 1} \qquad (6)$$

Where T_s is the sampling period, N is the parameter of the first-order filter on the derivative term, $K_p,\ K_i,\ K_d$ denotes the proportional, integral, and derivative gains of the PID controller, respectively.

Again, Equation (5) can be modified to form the following:

$$C(z) = \frac{b_0 + b_1 z^{-1} + b_2 z^{-2}}{a_0 + a_1 z^{-1} + a_2 z^{-2}} \qquad (7)$$

where the coefficients are as follows:

$$b_0 = K_p(1+NT_s) + K_i T_s(1+NT_s) + K_d N$$
$$b_1 = -\left(K_p(2+NT_s) + K_i T_s + 2K_d N\right), \quad b_2 = K_p + K_d N$$
$$a_0 = (1+NT_s), \ a_1 = -(2+NT_s), \ a_2 = 1 \qquad (8)$$

The Phase Shift PWM block employs the phase-shifted pulse width modulation technique in the PID controller's output signal. It sends the necessary pulse signal to the switching devices to stabilize the output voltage signal

IV. Parameters of the Proposed Design

In charging mode, the input voltage range is 400-450 V, while the output voltage range is 250-465 V. Correspondingly, the discharging mode input voltage range is 250–465 V, while the output voltage range is 400–450 V. Both charging and discharging modes have a nominal operating frequency of 1 MHz. The resonant frequency is set at 1 MHz. To step up the input voltage, the transformer turns ratio, n is set to $\frac{8}{9}$ according to (1). Load resistance can be calculated from $\frac{V_o^2}{P}$ equation, where V_o and P is the expected output voltage and power, respectively. From (2), (3), (4), and (5), the resonant parameters L_1, L_2, L_m, C_1, and C_2 can be calculated, yielding:

$$L_1 = 3.49\,\mu H,\ L_2 = 4.42\,\mu H,\ L_m = 21\mu H\ ,$$
$$C_1 = 7.26\,nF,\ C_2 = 5.74\,nF \quad (9)$$

V. Simulated Results

The performance of the designed converter has been assessed using GaN, SiC, and Si-based switching devices. PLECS Standalone software has been used to simulate the entire system. The following subsections explain the performance of these devices.

A. *GaN System's E-mode GaN HEMT based CLLLC Converter*

GS66508T of GaN Systems has been used as a GaN switching device in this work. The GS66508T is a 650 V, 30 A enhancement-mode GaN-on-silicon power transistor. It offers a very high switching frequency (> 10 MHz), and zero reverse recovery loss. Fig. 5 illustrates the simulated waveforms of the converter with this device in charging mode. It is obvious that the switches achieve ZVS turn-on. In discharging mode, the circuits produce similar experimental results because the circuit structures are symmetrical.

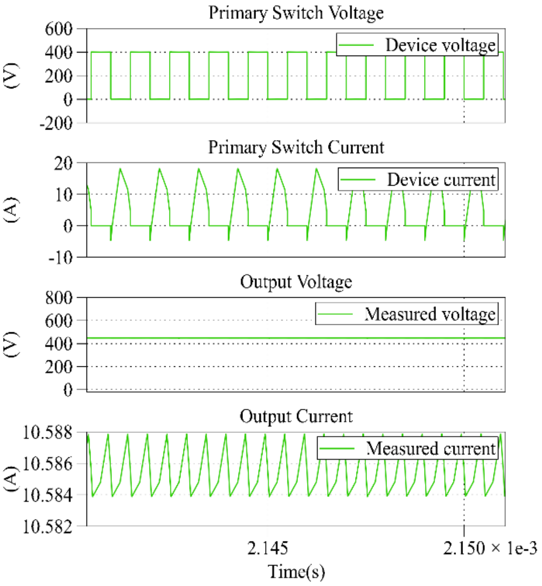

Fig. 5. Simulated waveforms of the converter with GaN device

B. *Cree's E-mode Planar SiC MOSFET based CLLLC Converter*

The n channel enhancement mode planar MOSFET model C3M0060065D from Cree Inc. has been used as a SiC switching device for this work. This 650V, 29A SiC MOSFET has a high blocking voltage with a low on-resistance, fast switching with low capacitances, and a fast intrinsic diode with a low reverse recovery (Qrr). The simulated waveforms in charging mode with this SiC device are shown in Fig. 6.

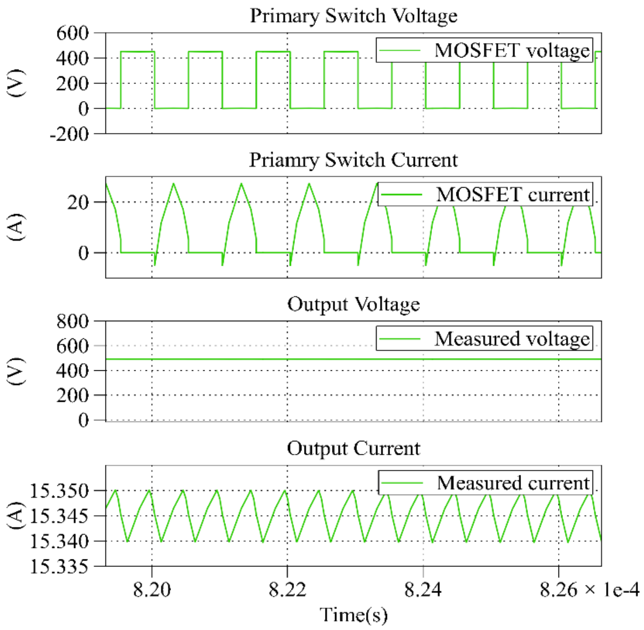

Fig. 6. Simulated waveforms of the converter with Planar SiC device

The waveforms demonstrate the switching device's ZVS. The output voltage and current are higher than the previous GaN device. Similar waveforms result in the converter's discharging mode.

C. *ROHM Semiconductor's Trench Structure SiC MOSFET based CLLLC Converter*

SCT3060AR from ROHM semiconductor is a 650V, 39A SiC MOSFET with a trench gate structure that is optimized for high-efficiency server power supply, solar power inverters, and EV charging stations. ROHM, a SiC

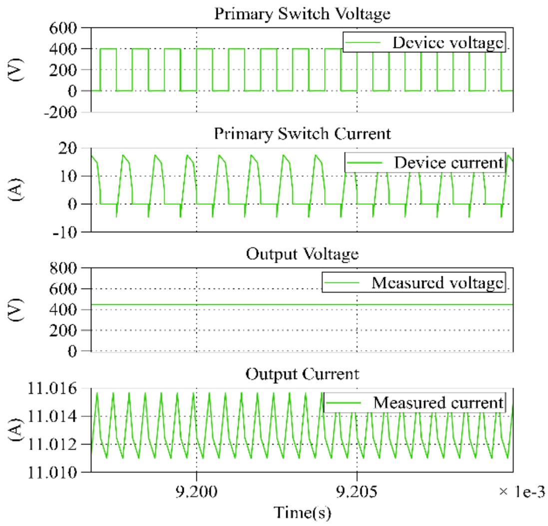

Fig. 7. Simulated waveforms of the converter with Trench-type SiC device

technology pioneer and industry leader, was the first to mass-produce trench-type MOSFETs, which improve efficiency while reducing power consumption over conventional SiC MOSFETs. Fig. 7 depicts the converter performance with this device in charging mode. Based on the waveforms, it is clear that this device also exhibits ZVS turn-on. In discharging mode, the converter yields similar results.

D. Infineon's Si Power Transistor based CLLLC Converter

Infineon Technologies' SPP20N60C3 Si power transistor has a 650V, 20.7 A rating. This device has a very low gate charge, a high peak current capability, and better transconductance. Fig. 8 depicts the performance of the designed converter when using this device in charging mode.

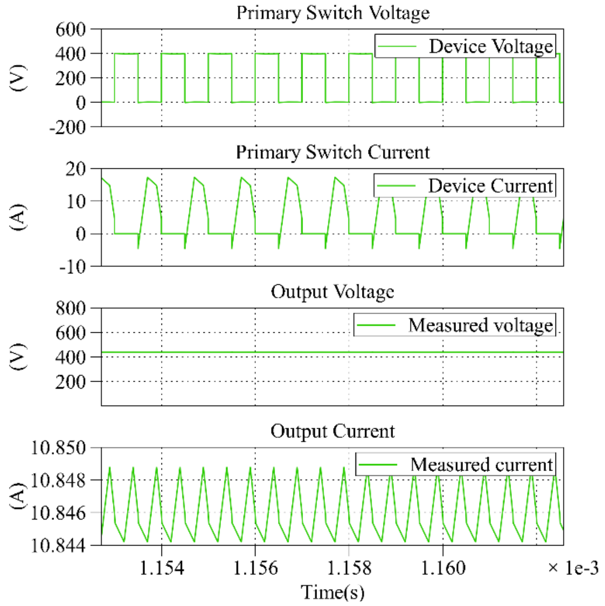

Fig. 8. Simulated waveforms of the converter with Si Power Transistor

In this case, too, the switching device provides ZVS turn on. In discharging mode, the converter performance is similar.

E. ROHM's Field Stop Trench IGBT based CLLLC Converter

ROHM's RGW60TS65DHR is a 650V 30A field stop trench IGBT. It has a low switching loss and a built-in fast recovery diode (FRD) for reverse conduction. Fig. 9 shows

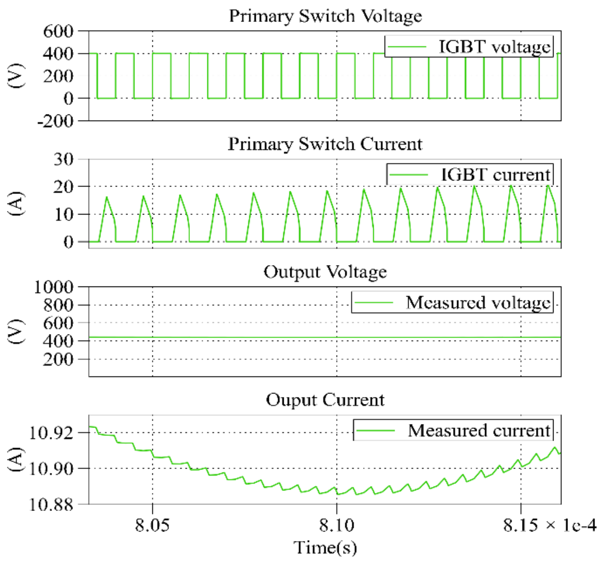

Fig. 9. Simulated waveforms of the converter with Si IGBT

the converter's performance while using the device in charging mode. It ensures that ZVS is also turned on. In the discharging mode, the converter performs similarly.

VI. RESULT ANALYSIS

Fig. 10 summarizes the comparisons of several switching devices utilizing the developed CLLLC converter.

(a)

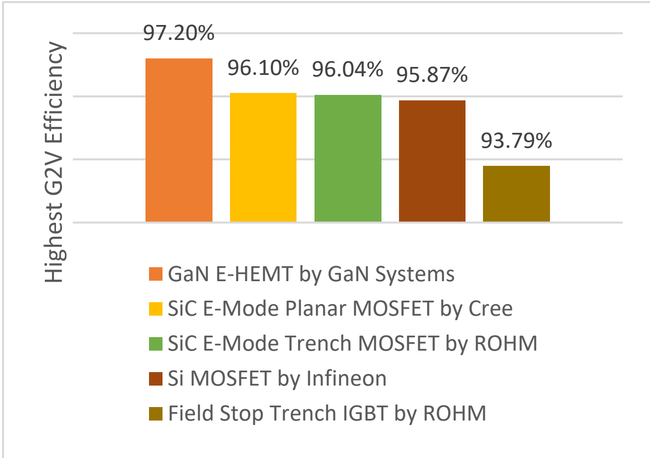

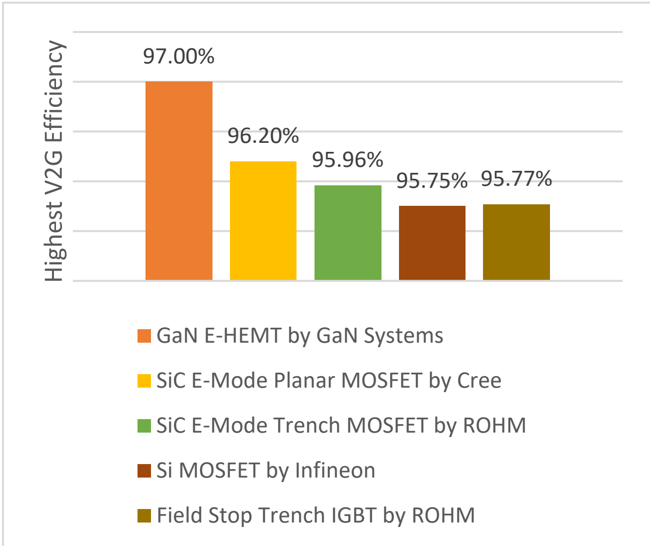

(b)

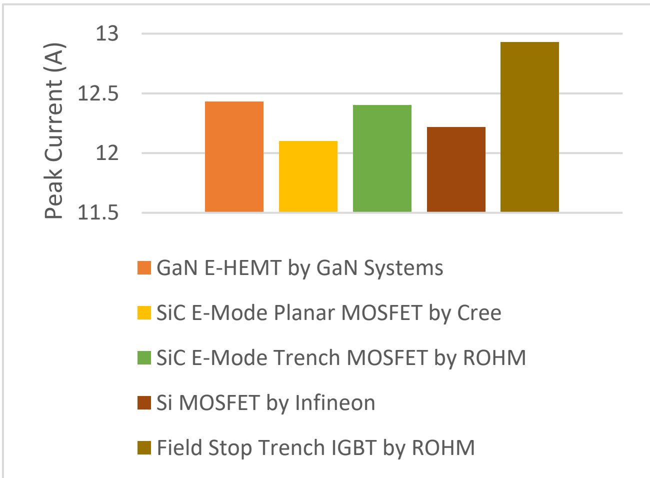

(c)

Fig. 10. Comparison of (a) Highest G2V Efficiency, (b) Highest V2G Efficiency (c) Peak Output Current

As shown in Fig. 10 (a), the designed CLLLC converter has the highest G2V efficiency (97.2 percent) while using GaN as a switching device. SiC and Si MOSFETs-based designs perform slightly worse than GaN devices, while Si IGBT-based design performs the worst. The scenario in charging mode or V2G mode is similar to that in discharging mode or G2V mode, as illustrated in Fig. 10. (b). Fig. 10(c) depicts the peak output current provided by the designed converter when various switching devices are used. Cree's SiC and ROHM's IGBT achieved the lowest and highest peak output currents, respectively. So overall, a GaN-based switching device can provide the optimized solution for the designed converter. Furthermore, in terms of highest G2V efficiency, highest V2G efficiency, and peak output power, this converter outperforms both the GaN-based CLLLC converter proposed in [19] and the GaN-based multi-resonant converter proposed in [20], as shown in Table I..

TABLE I. PERFORMANCE COMPARISON

Criteria	[19]	[20]	This work
Highest G2V Efficiency (%)	95.2	92.2	97.2
Highest V2G Efficiency (%)	95.7	92	97
Peak Output Power (kW)	1	0.4	5

VII. Conclusion

This paper describes the detailed design approach for the bidirectional CLLLC resonant converter. The converter is designed and simulated for a 5 kW power rating with an input voltage range of 400-450V DC and an output voltage range of 250-465V DC at 1 MHz switching frequency. High efficiency and bidirectional power flow are possible with this converter. The CLLLC architecture assures soft switching of both primary and secondary switches, considerably lowering switching loss at this MHz situation. This paper also includes a thorough analysis of the proposed converter as well as a comparison of the switching devices available for this converter. GaN-based CLLLC converters have the highest efficiency of any available switching device due to their low switching loss and zero reverse recovery loss. SiC-based designs are slightly less efficient, and Si-based designs are the least efficient. Peak efficiencies for this GaN-based CLLLC converter at full load are 97.2 percent for the charging mode and 97 percent for the discharging mode. Because of the converter's high frequency (1 MHz) operation, the size of the passive storage components is also small. As a result, this converter can attain a high-power density. So, this bidirectional CLLLC converter based on GaN device could be highly effective for EV applications due to its high performance.

References

[1] L. Tarisciotti, A. Costabeber, L. Chen, A. Walker, and M. Galea, "Current-Fed Isolated DC/DC Converter for Future Aerospace Microgrids," *IEEE Trans. Ind. Appl.*, vol. 55, no. 3, pp. 2823–2832, 2019, doi: 10.1109/TIA.2018.2889845.

[2] R. Bosshard and J. W. Kolar, "Multi-Objective Optimization of 50 kW/85 kHz IPT System for Public Transport," *IEEE J. Emerg. Sel. Top. Power Electron.*, vol. 4, no. 4, pp. 1370–1382, 2016, doi: 10.1109/JESTPE.2016.2598755.

[3] B. Li, Q. Li, and F. C. Lee, "A novel PCB winding transformer with controllable leakage integration for a 6.6kW 500kHz high efficiency high density bi-directional on-board charger," *Conf. Proc. - IEEE Appl. Power Electron. Conf. Expo. - APEC*, pp. 2917–2924, 2017, doi: 10.1109/APEC.2017.7931111.

[4] F. Krismer and J. W. Kolar, "Efficiency-optimized high-current dual active bridge converter for automotive applications," *IEEE Trans. Ind. Electron.*, vol. 59, no. 7, pp. 2745–2760, 2012, doi: 10.1109/TIE.2011.2112312.

[5] B. Pal, S. S. Saha, and P. Biswas, "Power Electronics—EV Battery Charging," in *Electric Vehicles: Modern Technologies and Trends.*, 1st ed., J. B. Patel, N., Bhoi, Akash Kumar, Padmanaban, Sanjeevikumar, & Holm-Nielsen, Ed. Springer, Singapore, 2021, pp. 73–93.

[6] B. Zhao, Q. Song, W. Liu, and Y. Sun, "Overview of dual-active-bridge isolated bidirectional DC-DC converter for high-frequency-link power-conversion system," *IEEE Trans. Power Electron.*, vol. 29, no. 8, pp. 4091–4106, 2014, doi: 10.1109/TPEL.2013.2289913.

[7] P. He and A. Khaligh, "Comprehensive Analyses and Comparison of 1 kW Isolated DC-DC Converters for Bidirectional EV Charging Systems," *IEEE Trans. Transp. Electrif.*, vol. 3, no. 1, pp. 147–156, 2017, doi: 10.1109/TTE.2016.2630927.

[8] Y. Tang, J. Lu, B. Wu, S. Zou, W. Ding, and A. Khaligh, "An Integrated Dual-Output Isolated Converter for Plug-in Electric Vehicles," *IEEE Trans. Veh. Technol.*, vol. 67, no. 2, pp. 966–976, 2018, doi: 10.1109/TVT.2017.2750076.

[9] H. T. Chang, T. J. Liang, and W. C. Yang, "Design and Implementation of Bidirectional DC-DC CLLLC Resonant Converter," *2018 IEEE Energy Convers. Congr. Expo. ECCE 2018*, pp. 2712–2719, 2018, doi: 10.1109/ECCE.2018.8557697.

[10] Z. M. Dalala, Z. U. Zahid, O. S. Saadeh, and J. S. Lai, "Modeling and Controller Design of a Bidirectional Resonant Converter Battery Charger," *IEEE Access*, vol. 6, no. c, pp. 23338–23350, 2018, doi: 10.1109/ACCESS.2018.2830321.

[11] Z. Lv, X. Yan, Y. Fang, and L. Sun, "Mode analysis and optimum design of bidirectional CLLC resonant converter for high-frequency isolation of DC distribution systems," *2015 IEEE Energy Convers. Congr. Expo. ECCE 2015*, pp. 1513–1520, 2015, doi: 10.1109/ECCE.2015.7309873.

[12] Z. Liu, F. C. Lee, Q. Li, and Y. Yang, "Design of GaN-Based MHz Totem-Pole PFC Rectifier," *IEEE J. Emerg. Sel. Top. Power Electron.*, vol. 4, no. 3, pp. 799–807, 2016, doi: 10.1109/JESTPE.2016.2571299.

[13] S. Zong, G. Fan, and X. Yang, "Double Voltage Rectification Modulation for Bidirectional DC/DC Resonant Converters for Wide Voltage Range Operation," *IEEE Trans. Power Electron.*, vol. 34, no. 7, pp. 6510–6521, 2019, doi: 10.1109/TPEL.2018.2875816.

[14] Y. Chu, A. Kumar, and Y. Ramadass, "Common-Mode EMI cancellation in full-bridge based isolated DC-DC Converters," *Conf. Proc. - IEEE Appl. Power Electron. Conf. Expo. - APEC*, pp. 284–291, 2021, doi: 10.1109/APEC42165.2021.9487124.

[15] T. Yu, G. Sicheng, and X. Shaojun, "Research on Open-loop Soft-start Strategy of CLLLC Bi-directional Resonant Converter," *Proc. - 2018 IEEE Int. Power Electron. Appl. Conf. Expo. PEAC 2018*, pp. 1–6, 2018, doi: 10.1109/PEAC.2018.8590641.

[16] J. Millan, P. Godignon, X. Perpina, A. Perez-Tomas, and J. Rebollo, "A survey of wide bandgap power semiconductor devices," *IEEE Trans. Power Electron.*, vol. 29, no. 5, pp. 2155–2163, 2014, doi: 10.1109/TPEL.2013.2268900.

[17] J. H. Jung, H. S. Kim, M. H. Ryu, and J. W. Baek, "Design methodology of bidirectional CLLC resonant converter for high-frequency isolation of DC distribution systems," *IEEE Trans. Power Electron.*, vol. 28, no. 4, pp. 1741–1755, 2013, doi: 10.1109/TPEL.2012.2213346.

[18] B. Yang, "Topology investigation for front end DC /DC power conversion for distributed power system," Virginia Polytechnic Institute and State University, 2003.

[19] A. M. Ammar, K. Ali, and D. J. Rogers, "A Bidirectional GaN-Based CLLC Converter for Plug-In Electric Vehicles On-Board Chargers," *IECON Proc. (Industrial Electron. Conf.*, vol. 2020-Octob, pp. 1129–1135, 2020, doi: 10.1109/IECON43393.2020.9254560.

[20] Y. F. Wang, B. Chen, Y. Hou, Z. Meng, and Y. Yang, "Analysis and Design of a 1-MHz Bidirectional Multi-CLLC Resonant DC-DC Converter with GaN Devices," *IEEE Trans. Ind. Electron.*, vol. 67, no. 2, pp. 1425–1434, 2020, doi: 10.1109/TIE.2019.2899549.